

Solution-Processed Metallic Nanowire Network for Wearable Transparent Thermal Radiation Shield

Genesis Higueros, Keyu Wang, Chenxi Sui, and Po-Chun Hsu*



Cite This: <https://doi.org/10.1021/acsnano.4c02093>



Read Online

ACCESS |



Metrics & More



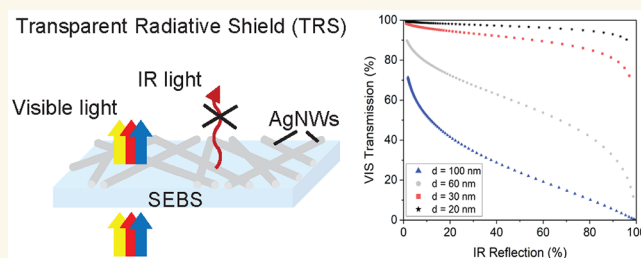
Article Recommendations



Supporting Information

ABSTRACT: Heating requirements for residential and commercial dwellings result in significant energy consumption and deleterious environmental effects. Personal radiative thermal management textiles regulate the wearer's body temperature by controlling the material's intrinsic optical properties. Passive heating textiles suppress radiative heat losses and therefore significantly reduce the energy consumption required for building heating systems. Guided by an optical theoretical approach, a transparent radiation shield (TRS) is designed based on silver nanowires (AgNWs) that can suppress human body heat with simultaneous visible light transmittance anticipated for practical fabrics. We experimentally demonstrated a TRS with large infrared light reflectance (low emissivity of 35%) and a visible (VIS) transparency value of 75% (400–800 nm). The results are well corroborated by the Mie scattering theory and the wire-mesh equivalent sheet impedance model, which provide fundamental mechanism understanding and guidance toward higher performance. The TRS is fabricated by a simple, solution-processing method with thermoplastic elastomer protective layers, granting notable stretching capabilities, mechanical robustness, and conformability to any body shape or object. The rigorous theoretical strategy enables the scalable synthesis of low-emissivity and visibly transparent textiles for personal thermal comfort.

KEYWORDS: personal thermal management, mid-infrared emissivity, nanofabrication, smart textiles, wearable electronics, passive radiative heating



In 2010, the building sector, which accounts for all private and nonprivate dwellings, contributed roughly 8.8 GtCO₂ emissions and 32% of final energy use.^{1,2} Additionally, energy demand is expected to double by 2050 while CO₂ emissions will see a 50–150% increase from the building sector, according to the Intergovernmental Panel on Climate Change. To mitigate such greenhouse gas emissions, personal thermal management textiles have been proposed and demonstrated to localize the heating and cooling on the human body rather than the entire building space, thereby minimizing the energy requirement and thermal inertia.^{3–7}

At rest, thermal radiation is a predominating part of human body heat loss (40–60%)⁷ due to the high emissivity of commercial textiles and human skin.⁵ By designing wearable textiles with low emissivity, reliance on heating, ventilation, and air conditioning (HVAC) systems for indoor heating will diminish, saving users significant energy use and financial costs. In addition to alleviating CO₂ emissions, personal thermal management wearables prevent medical emergencies and at times life-threatening cases such as frostbite and hypothermia resulting from prolonged duration in extremely cold temper-

atures. Personal thermoregulatory strategies will protect populations at large risk of experiencing cold injuries including but not limited to outdoor workers, unsheltered individuals, and persons with certain pre-existing health conditions such as arthritis.^{8,9}

To fabricate a practically viable wearable thermoregulatory textile, it is necessary to meet the following criteria: (i) The manufacturing approach must be scalable and potentially compatible with the existing textile industry.³ (ii) The material must be mechanically flexible, lightweight, nontoxic, breathable, washable, and robust.^{3,10} (iii) High performance in thermoregulation, minimal wear-and-tear, and low to no energy consumption are also valued. (iv) A personal thermal

Received: February 12, 2024

Revised: May 3, 2024

Accepted: May 9, 2024

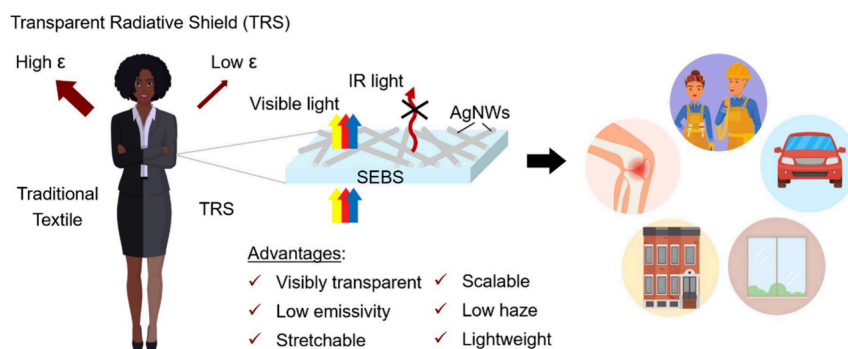


Figure 1. Transparent radiative shield (TRS) design concept and applications. A highly stretchable and scalable shield suppresses human body heat with limited aesthetic disruption to commercial textiles, which minimizes HVAC energy usage for multiple spaces and prevents cold-related injuries.

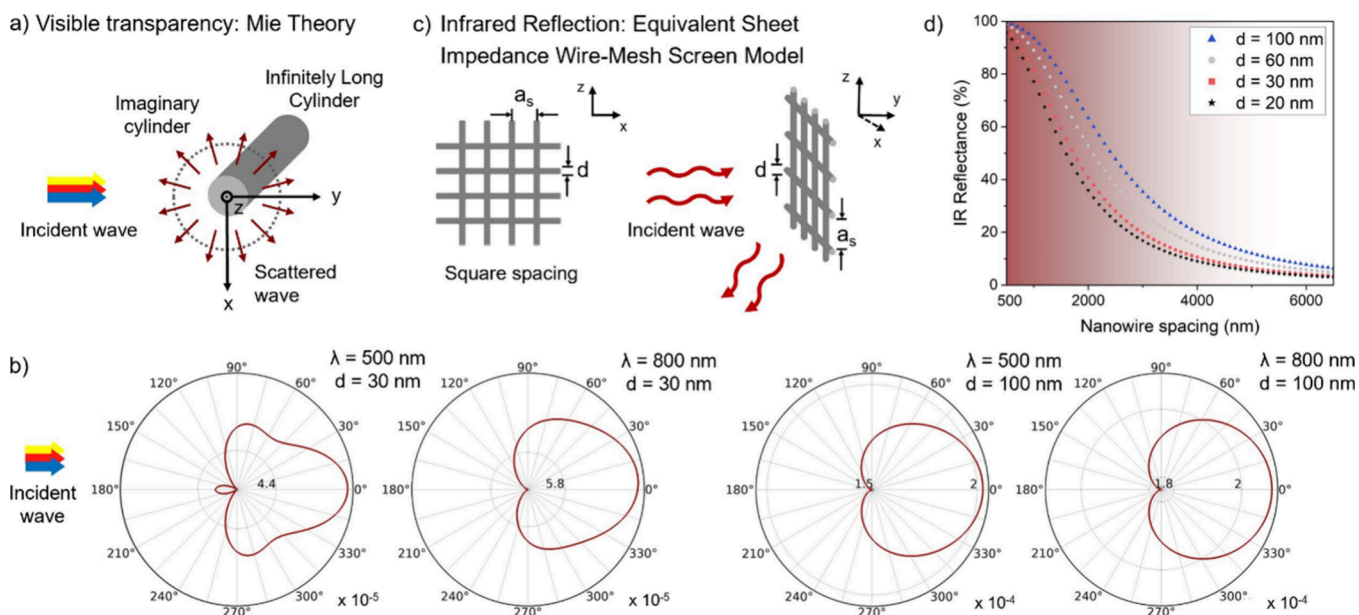


Figure 2. Theoretical consideration for the TRS design. (a) Mie theory schematics for single AgNW scattering. (b) Normalized far-field scattering (V/m) polar plot for a single AgNW with incident light approaching from the left (180°). Nanowires show strong forward scattering that is beneficial for total visible transmittance. (c) The wire-mesh screen model for the network's visible light transmittance and mid-IR light reflectance. (d) The mid-IR ($8\text{--}13\ \mu\text{m}$) reflectance as a function of nanowire spacing for various nanowire diameters. Ideal mid-IR reflectance occurs as the nanowire spacing nears $500\ \text{nm}$.

management textile must restrict its impact on aesthetics while maintaining its thermoregulatory properties because commercial garments are sold in a plethora of visible colors and patterns. After all, without these advanced requirements, a simple emergency survival blanket can already work as an effective thermal radiation shield, although it is apparently not ideal for everyday use.

Previous strategies for personal thermal management devices have involved metallic nanowires, metallic films, metamaterials, MXenes, structural polymers, oxide-metal-oxide films, and more.^{5,7,10–18} Recently, a focus on colorful fabrics has emerged to further improve on passive personal thermoregulatory textiles, demonstrating excellent performance in electromagnetic shielding and strong propagation of single-colored visible light.^{19–22} Strives have been made by the scientific community to enhance color visibility independent of the viewing angle. Such optical properties of colorful fabrics are inherently wavelength-dependent. Hence, the emissivity and solar absorption will alter between colors. To assume low emissivity for all colors in the visible spectrum, visibly

transparent infrared-reflective coatings have been produced.^{23–31}

Transparent thermal management textiles have been previously synthesized as wearable fabrics and window coatings, accomplishing energy savings from reduced energy use in HVAC systems.^{26–28} For instance, visible (VIS) transmittance up to 80% at $550\ \text{nm}$ was achieved for an oxide-metal-oxide nanomesh composite with emissivity below 20% for mid-infrared (mid-IR) wavelengths between 7 and $14\ \mu\text{m}$.²³ However, the previously mentioned criteria have not been met because cleanroom fabrication processes are still required for these prior reports.^{24,29,30} On the other hand, silver nanowires (AgNWs) on flexible substrates have demonstrated large visible transmittance of 78% and 83% at $550\ \text{nm}$ with scalable methods such as solution processing or spray coating, respectively, but these devices are designed specifically for building windows and do not stretch.^{27,28} Additional projects have incorporated silver nanowires for transparent wearable electronics, yet design parameters will require different criteria for conductive electrodes versus

passive electromagnetic shielding materials.^{25,32} Despite progress in translucent flexible textiles using metallic nanowires, a numerical approach for designing ultratransparent and low-emissive AgNW coatings for thermal management garments has yet to be discussed.

Herein, a visibly transparent and passive heating wearable technology is demonstrated using a solution-processed metallic nanowire network as the transparent radiation shield (TRS) shown in Figure 1. In comparison to the highly emissive traditional textiles, the TRS limits mid-IR thermal radiation while simultaneously permitting transmission of VIS light. The AgNW network, its supporting substrate, and the topcoat protective layer can all be fabricated by simple thin-film casting methods (e.g., drop cast, blade cast, spin-coating, and spray coating), which minimize resource requirements and abstains from cleanroom processes. The TRS achieves more than 75% visible transmittance at emissivity below 35%, and its optical performance is compared to the previously discussed literature on visibly transparent and infrared reflective coatings in Table S1. Elongation capability and solution processability of the devices are also identified, illustrating the improvements established by the TRS. Furthermore, the TRS is inexpensive, lightweight, highly stretchable, and low in haze. As a result of its numerous benefits, the TRS can be applied to multiple objects, such as uniforms for outdoor workers, car tints, thermally insulated windows for buildings, and persons prone to cold-related injuries.

The key to achieving both extreme visible transparency and low thermal emissivity lies in the different light–matter interactions for VIS and mid-IR light. Consider a AgNW network with a diameter of 30–100 nm and average wire-to-wire spacing of less than 2 μm . When visible light ($\lambda = 400\text{--}700\text{ nm}$) shines onto the AgNW network, we can expect two sources of light–matter interaction: the single AgNW and the wire-to-wire spacing. For a single AgNW, the scattering cross section, light propagation trajectory, and angular distribution can be well-described by Mie theory, which predicts mostly forward-scattering light transmission at this small nanowire diameter. The backscattering portion results in visible opacity, and the high-angle forward scattering accounts for the haze. The empty space between the AgNWs is 100% in visible light transmittance, because the dimension is much larger than the wavelength. For mid-IR ($\lambda = 4\text{--}30\ \mu\text{m}$), both the AgNW diameter and the network spacing are now small in comparison, so it acts as a wire-mesh screen with a waveguide cutoff wavelength smaller than that of the incident mid-IR, resulting in large reflectivity and therefore low absorptivity (assuming zero transmittance). According to Kirchhoff's law, this low absorptivity is equivalent to low emissivity.

MieSolver is employed to predict visible transmittance ($\lambda = 400\text{--}800\text{ nm}$) of an infinite cylinder, as shown in Figure 2a.³³ Incident light shines on a single silver nanowire with infinite length and an opaque core perpendicular to its z -axis. A detailed description of the problem statement and Mie series solution is presented in Supporting Information Note 1. Far-field approximation is used to calculate the visible wave propagation of nanowire mesh screen.^{34,35} As described by eq 1, the transmittance intensity across a material's thickness is assumed to follow the Beer–Lambert law, which is proportional to the incident intensity and the exponential term containing the scattering coefficient (α_{scat}) and thickness (t). For simplification purposes, a single layer of AgNWs is assumed.

$$I = I_0 e^{-\alpha_{\text{scat}} t} \quad (1)$$

Visible transmission computation requires the concentration of nanowires (N), which is approximated by the corresponding wire-mesh screen porosity (ρ), whose nanowire spacing (a_s) is chosen to be between 500 and 10 500 nm. Derivation for nanowire concentration is defined in Supporting Information Note 2. Additionally, the scattering coefficient is characterized by the forward scattering cross section (σ_{scat}) and nanowire concentration (N).

To further prove the large visible transmittance for the AgNW mesh network, COMSOL simulations are performed according to Mie theory to calculate the angle-resolved scattered light distribution for a single infinite cylinder. Figure 2b compares the scattered wave of a single AgNW with diameters of 30 and 100 nm at the incident wavelengths (λ_{inc}) of 500 and 800 nm. Forward scattering is demonstrated for both diameters and wavelengths. However, the normalized amplitude for 100 nm-diameter AgNWs is wider and relatively high in value (10-fold when compared to 30 nm-diameter AgNWs), which will contribute to haze hindering transmission of VIS light. COMSOL simulations for alternative diameters ($d = 20$ and 60 nm) at identical incident wavelengths are shown in Figure S1, illustrating similar forward scattering polar plots.

The mid-IR (8–13 μm) property is based on the equivalent sheet impedance wire-mesh screen model (Figure 2c).³⁶ The model assumes square apertures with a maximum pore size dictated by the frequency of interest. Briefly, by calculating the equivalent sheet impedance of the wire mesh, one can compute the reflectance coefficients of the transverse-electric and transverse-magnetic fields of the wave function defined in Supporting Information Note 1. Nanowire spacing (a_s) and diameter (d) are two parameters of the wire-mesh screen model investigated to predict mid-IR reflection. As mentioned earlier, Kirchhoff's law, at thermodynamic equilibrium, states emissivity (ϵ) of a material equals absorptivity (A). Therefore, high reflectance is achieved with low-emissive material such as metallic nanowires, as shown in eq 2. Hence, AgNWs are investigated as a possible transparent radiation shield.

$$\epsilon = A = 1 - R - T = 1 - R \quad (2)$$

Based on these theoretical models, we can predict the relationship between visible transmittance and mid-infrared emissivity as a function of nanowire diameter and spacing. From our Mie theory predictions, extreme visible transmittance is expected for nanowires with a small diameter (<30 nm) and nanowire spacing > λ_{inc} . On the other hand, mid-IR reflection changes minimally for all nanowire diameters investigated with respect to nanowire spacing, as illustrated in Figure 2d. Instead, nanowire spacing plays a significant role in influencing the mid-IR reflectance. As expected, large pore size ($a_s > 4000\text{ nm}$) will result in almost no reflection of mid-IR radiation. Hence, the graded red region represents an ideal nanowire spacing for large mid-IR reflectance. The multi-spectral computation above allows us to investigate both the VIS transmittance and mid-IR reflection for any given nanowire spacing and AgNW diameter and serves as a powerful predicting tool to guide fabrication and manufacturing.

For wearable applications, a robust yet flexible substrate for AgNWs is necessary for defense against wear-and-tear, environmental conditions, and common sanitization methods. For radiative heat management, in particular, this protective

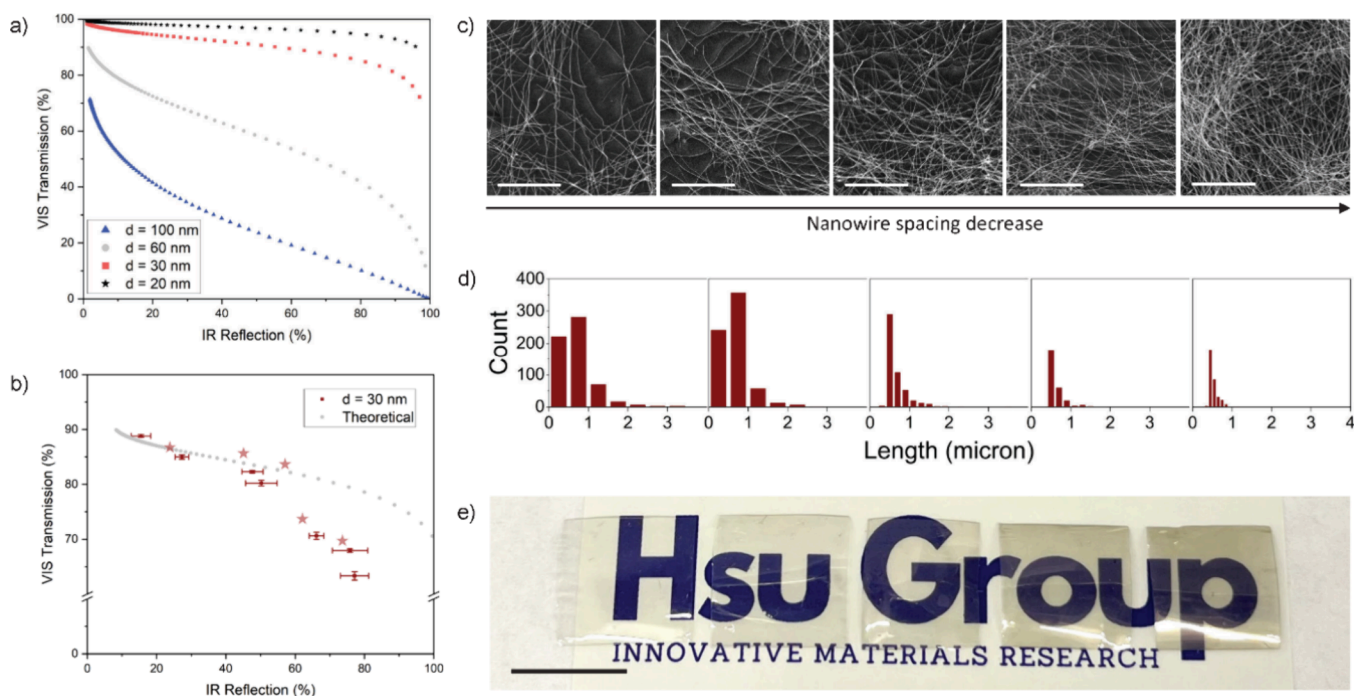


Figure 3. Fabrication proposal for single-layer AgNW network. (a) VIS transmittance for multiple AgNW networks varying in diameter is compared. (b) Experimental data points of AgNW networks with various nanowire spacings. (c) SEM images, (d) nanowire spacing histograms, and (e) optical images of starred data points illustrate lower visibility for multilayer AgNW networks. The scale bar is $5 \mu\text{m}$ for all SEM images and 10 mm for the optical image. Photo credit: Genesis Higueros

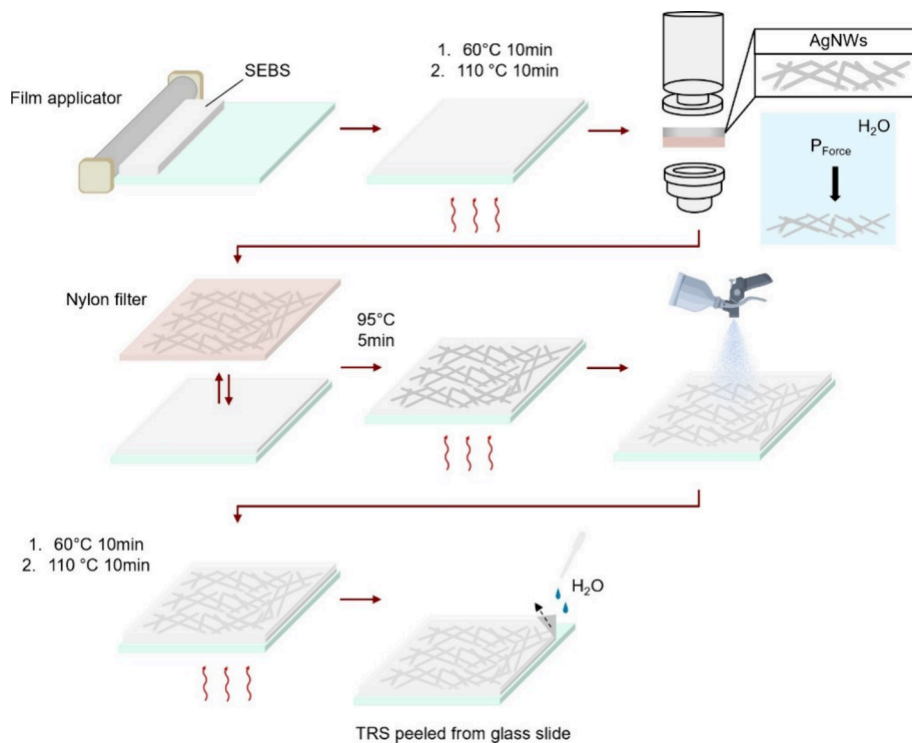


Figure 4. Synthesis of the TRS by vacuum filtration of AgNWs and spray deposition of a SEBS protective film.

layer should be transparent in mid-IR, so that the low-emissivity nature of AgNWs can be used entirely. To this end, we chose polystyrene-*block*-poly(ethylene-*ran*-butylene)-*block*-polystyrene (SEBS) as the underlayer. In addition to mid-IR transparency, solution-processed SEBS is highly stretchable and flexible, capable of taking any form. Its mechanical and

optical properties are dictated by the polymer chain composition in which polybutylene and polyethylene groups contribute to the elasticity and mid-IR transparency of SEBS, respectively.^{37–40} The physical cross-links of styrene groups are rigid, and the benzene ring results in large intrinsic mid-IR absorption coefficients. Therefore, a low content of polystyrene

in SEBS is required. As a comparison, polydimethylsiloxane (PDMS) elastomers absorb most wavelengths in the mid-IR regime, which makes it a nonsuitable candidate for the TRS, although it is frequently used in wearable materials research. To investigate the inhibition of AgNW reflectivity by polymer substrates and topcoats, Figure S2 compares the mid-IR reflectances of SEBS, PDMS, and polyurethane (PU). The supporting figure also demonstrates the robustness of materials by tensile testing, proving SEBS to be the ideal contender. On the other hand, mid-IR absorbance for SEBS is thickness-dependent and can be minimized. SEBS empirical influence on the optical properties of AgNWs is accounted for in the simulation data (i.e., measured reflectance and transmission from the pristine SEBS specimen are removed).

Determined by our theoretical predictions, the metallic nanowire mesh screen used for the TRS must be small in diameter (<30 nm) and pore size (<4000 nm), and it must be fabricated as a single-layer, continuous network in which infinite nanowire lengths are assumed. Figure 3a demonstrates the significance of employing ultrathin AgNWs. VIS transmittance is plotted against mid-IR reflectance for several nanowire diameters (20, 30, 60, and 100 nm) and nanowire spacings between 500 and 10500 nm. As illustrated, the visible transmittance of AgNWs with a diameter < 30 nm remains above 70% for all mid-IR reflection and nanowire spacing values. Therefore, a diameter below 30 nm is recommended by our simulations. As our theoretical approach assumes infinitely long nanowires, AgNWs with small diameters and long lengths are the ideal parameters for high performance in shielding efficiency and VIS transmittance. However, it is challenging to synthesize AgNWs with relatively long lengths (>20 μm) at smaller diameters (<20 nm), compromising the mid-IR reflectance. Tao et al. have previously demonstrated long nanowire lengths to improve visible transmittance and reduce VIS haze.⁴¹ Hence, length plays an important role in achieving high VIS transmittance and is a parameter that should be investigated further in the future.

VIS transmission for a larger diameter varies drastically across different nanowire spacings. The influence of cylinder diameter on haze results in a decrease in VIS transmittance for diameters > 60 nm, as previously illustrated by COMSOL simulations. Therefore, for thick AgNWs with a 100 nm diameter, VIS transmittance will have to be sacrificed to achieve high mid-IR reflectance. In this work, AgNWs with dimensions of 30 nm in diameter and 20 μm in length are employed.

To achieve a single-layer AgNW mesh, a vacuum filtration procedure similar to ref 25 is used. A solution of low-concentrated AgNWs in water solvent is vacuum filtered in a Buchner funnel flask with a nylon filter of pore size 0.22 μm . Thoroughly mixing the AgNW solution prior to filtration allows for uniform distribution of nanowires, and the hydraulic pressure assists the bonding of nanowire junctions. Once dried, the AgNW network is placed firmly above a premade SEBS thin film as illustrated in Figure 4. The nylon filter is peeled to transfer the AgNWs onto SEBS, and the composite is heated to 95 $^{\circ}\text{C}$. A top layer of SEBS solution is spray deposited over the exposed AgNWs to preserve the optical performance of nanowires from weathering conditions as well as common sterilization procedures, as seen in Figure 4. AgNW network pore size is dictated by nanowire concentration for each specimen. The TRS is ultimately formed via removal of the SEBS–AgNWs–SEBS composite from its glass substrate with

merely a few droplets of water. A SEBS film is prepared by drop-casting a solution of 20 wt % SEBS in toluene onto a glass slide (bottom substrate). As illustrated in Figure S3a, a film applicator disperses the SEBS solution before undergoing heat treatments for 10 min each at 60 and 110 $^{\circ}\text{C}$ following a similar process performed by ref 42.

The TRS can be manufactured in multiple ways, as presented in Figure S3b. Solution-processing of AgNW networks such as spin-coating, spray coating, and vacuum deposition are common fabrication methods for transparent wearable technology.^{18,31} The sole limitation to specimen size is determined by glass substrate dimensions, and synthesis procedures require no cleanroom processing. The top protective layer may also be added by a blade casting method rather than spray coating, proving the versatility of synthesizing TRS specimens (Figure S3c). The device may be coated onto any commercial textile for passive suppression of human body radiation with minimal impact to aesthetics.

RESULTS/DISCUSSION

VIS transmittance and mid-IR reflectance for several TRS specimens varying in nanowire concentration are plotted in Figure 3b. Experimental data points agree well with the theoretical curves for mid-IR reflectance below 60% in which VIS transmittance is more than 80%. For mid-IR reflectance values above 60%, the VIS transmittance slightly diminishes as a direct result of bilayer formation of AgNW networks. Theoretical predictions assume a single layer of AgNW network for all nanowire spacings. However, the assumption does not hold true for nanowire spacings < 900 nm because synthesis is challenging with the current scalable fabrication methods. Bilayer formation of AgNW networks can be seen in Figure 3c and is further discussed later. As illustrated, the TRS demonstrates high mid-IR reflectance (low emissivity of 35%) and a VIS transmission of 75%. Shielding effectiveness values for AgNWs in previous literature have ranged between 70% and 80%.^{23,27–29} The theoretical model presented here will serve as a valuable performance prediction tool for further fabrication method development.

The star data points represent five individual TRS specimens, and their respective scanning electron microscopy (SEM) images are shown in Figure 3c. SEM images provide qualitative information on the uniformity of AgNW distribution in addition to average nanowire spacing. As pore size decreases, mid-IR reflectance of the AgNW mesh increases. The nanowire spacing histograms for each specimen shown in Figure 3d further demonstrate the statistical decrease in the average aperture size. Porosity is also calculated to decrease with smaller nanowire spacings, as seen in Figure S4. SEM images were postprocessed using ImageJ software, and threshold images along with elliptical areas used to compute average nanowire spacings are also shown. Nanowire spacings with an approximate diameter below 500 nm are ignored for all histogram figures since this is the minimum wavelength cutoff for the VIS regime (transmission of VIS light becomes 0%). Optical images of all five TRS specimens are shown in Figure 3e, which further shows how the bilayer formation inhibits the VIS transmittance of our group logo. SEM images demonstrate bilayer formation of AgNW networks at high concentrations. Our theoretical simulations assume a single-layer nanowire network. However, an increase in nanowire density reduces pore spacing until a threshold is reached in which multiple layers of AgNWs are formed, and a single AgNW network layer

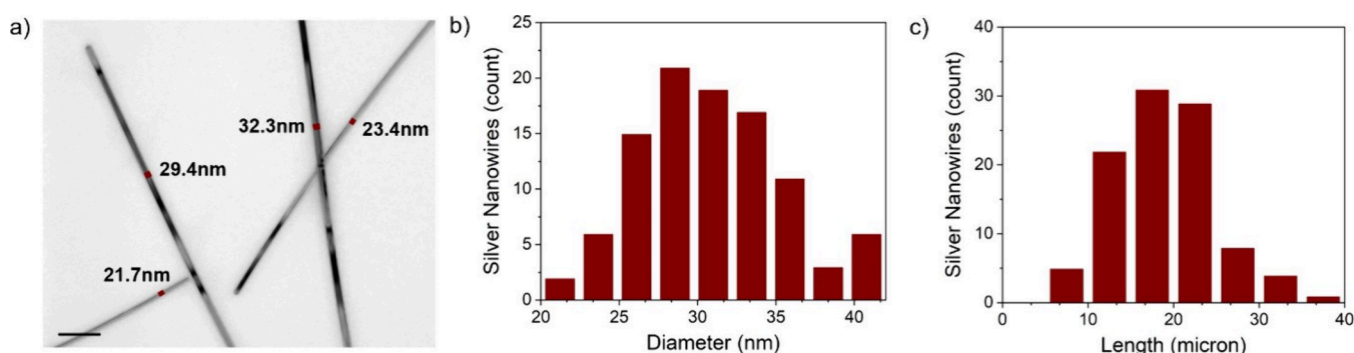


Figure 5. AgNW statistics. (a) TEM images of silver nanowires. The scale bar is 200 nm. (b) Diameter histogram for AgNWs measured from TEM images. (c) Length histogram for AgNWs on a SEBS substrate taken from optical images.

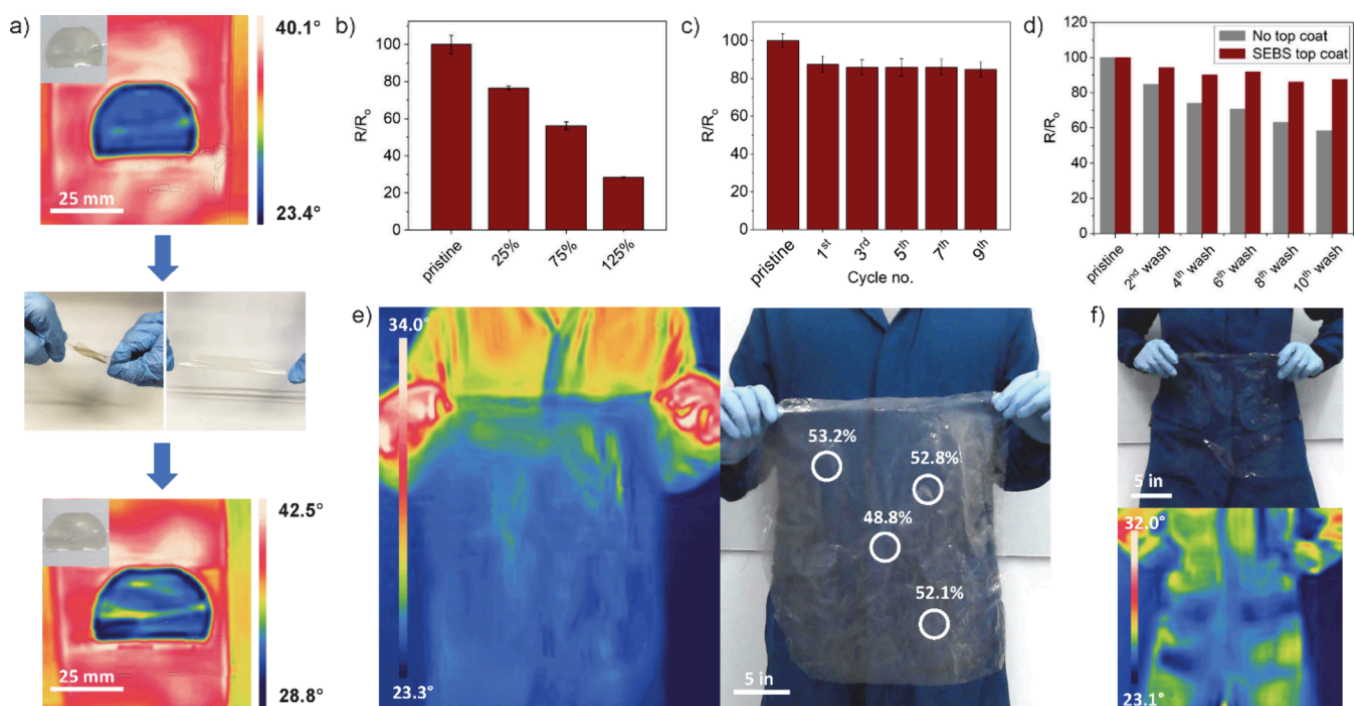


Figure 6. Mid-IR reflection performance for the TRS. (a) Thermal image of a TRS specimen before and after undergoing twisting and elongation. (b) Normalized mid-IR reflectance for a single TRS specimen at alternate elongation states of up to 125%. (c) Cyclic stretching of a TRS sample. (d) Wash tests performed on a TRS specimen and a sample with no top protective coat. SEBS top layer preserves the AgNW network. (e) Thermal image of a 15 in. \times 15 in. TRS specimen with four arbitrary locations chosen for mid-IR reflection measurement. (f) Thermal image of a pristine SEBS sample for comparison.

can no longer be achieved and assumed. Nevertheless, the theoretical model points out the importance of developing a fabrication method to achieve a single-layer AgNW network that can further boost the performance of the transparent radiation shield.

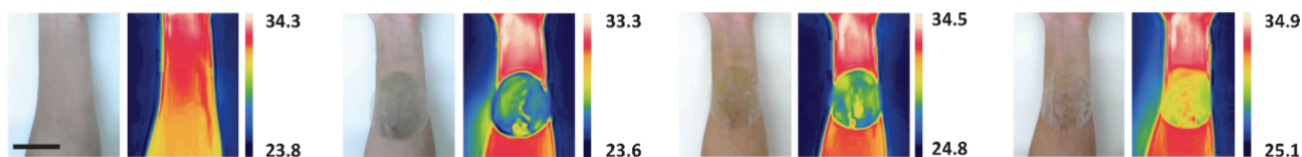
Length statistics for AgNWs were analyzed by optical images with 100 individual nanowires measured. Statistical analysis of AgNW diameter was assisted by transmission electron microscopy (TEM), as seen in Figure 5a. Figure 5b and c demonstrate a diameter mode of roughly 28 nm and a length mode of 18 μ m, respectively.

Mechanical robustness of the TRS was analyzed by cyclic stretching tests, laundry tests, and tensile tests. As observed in Figure 6a, the emissivity of a single TRS specimen remains low after undergoing stretching and twisting. To further ensure the shielding effectiveness of nanowire mesh is not impacted when stretched, the TRS devices undergo mid-IR measurements at

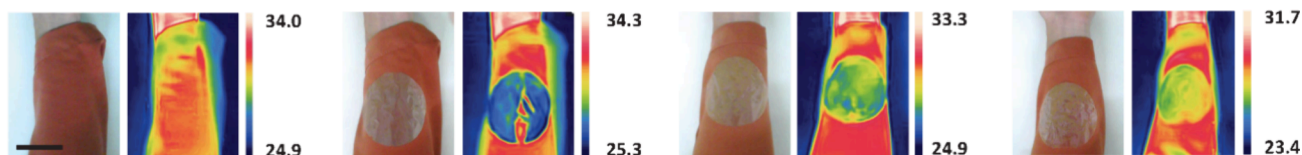
several elongation values revealed in Figure 6b. At 50% elongation, the TRS loses a portion of its shielding effectiveness. A decrease in mid-IR reflectance is predicted, as stretching results in an increase in nanowire spacing. SEM images were captured to ensure our hypothesis, and results can be seen in Figure S5 demonstrating an increase in nanowire spacing when samples are elongated. Nonetheless, poststretch measurements remain unaltered after 10 cycles, as illustrated in Figure 6c. This stretchability can be understood by the network deformation that avoids direct extreme tensile strain to individual nanowires. Additionally, the SEBS substrate assists in the reconnection of AgNW junctions poststretching.

Vigorous wash tests were performed to show the necessity of a SEBS protective layer. From experimental results, introducing a SEBS topcoat preserves AgNW shielding effectiveness, as illustrated in Figure 6d. After 10 cycles, normalized mid-IR reflectance remains >85%, while a TRS specimen with no

a) Bare forearm



b) 20% Spandex, 80% polyester



c) 100% Cotton

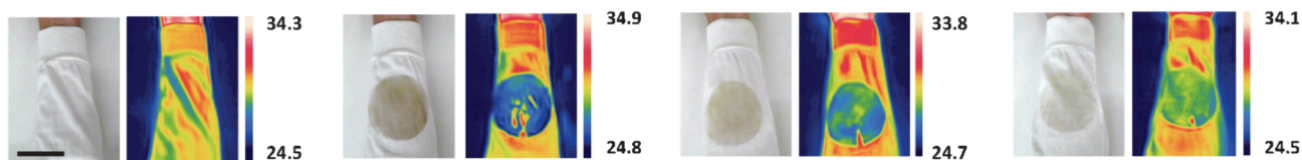


Figure 7. TRS improves human body heat suppression with minimal aesthetic disruption. Thermal camera and photographic images of (a) a bare forearm, (b) combined 80% polyester/20% Spandex cloth, and (c) 100% cotton with TRS specimens having alternate nanowire spacing (pore size increases from left to right). The scale bar is 50 mm for all thermal and optical images.

protective topcoat falls below 60%. Finally, a large TRS specimen (15 × 15 in.) is displayed in Figure 6e to demonstrate the scalability of spray-coating fabrication methods. Four arbitrary areas on the TRS specimen were measured for mid-IR reflectance and illustrate small standard deviation within a sample. A pristine SEBS specimen is shown in Figure 6f for comparison. Thermal images prove that mid-IR reflectance is caused by the AgNW network and not by the SEBS substrate.

Tensile testing was performed on four TRS samples and one pristine SEBS specimen. The average ultimate tensile strength was measured as 4.7 MPa, which is within range from previously reported commercial SEBS.^{37,43} Young's modulus was found to be 0.08 MPa. Stress versus strain curves for all specimens are displayed in Figure S6. The gray bar indicates the current commercial standard for the elongation of a pure cotton garment, demonstrating SEBS' outstanding stretching abilities. Additionally, Table S2 presents detailed information about the mechanical properties of each individual sample. To further demonstrate the stability of the TRS, mid-IR performance was investigated for specimens exposed to UV light for 2 weeks, representing approximately 1 year of natural sunlight. Figure S8 presents the degradation results for every 4 days of exposure and exhibits no significant change to the shielding effectiveness of TRS specimens. Supporting Information Videos 1–3 illustrate the flexibility and elastic stretching capabilities of the TRS.

The TRS specimens with alternate nanowire spacing passively heat a researcher's forearm in Figure 7a. In comparison to an 80% polyester textile mixed with Spandex (Figure 7b) and a garment made of 100% cotton (Figure 7c), the TRS displays improved shielding effectiveness while simultaneously allowing VIS light transmission from colorful fabrics. Nanowire spacing increases for TRS devices left to right for all images in Figure 7. Extreme low porosity (<1.8 μm

nanowire spacing) improves shielding effectiveness with a trade-off in VIS transmittance. Hence, an aperture size of approximately 1.8 μm is the optimal dimension for TRS specimens. For AgNWs with relatively large diameters (>60 nm), the compromise between VIS transmittance and mid-IR reflectance is strong. Our numerically guided theory suggests this relationship is less impactful for small diameters (<30 nm), in which VIS transmission remains above 75% for all samples varying in AgNW concentration.

The TRS promises high-performance visible transmission and human body heat suppression with an inexpensive and scalable manufacturing procedure. The cost to fabricate 1 kg or 1 × 1 m² of TRS is analyzed using OpenLCA software and found to be only \$4.34 (Table S3). Calculation of AgNWs and TRS net cost is discussed in detail in Supporting Information Note 4. Although AgNWs cost \$1046.79 per kg (Table S4), the TRS requires only a minuscule amount based on a single-layer AgNW mesh with 1.8 μm nanowire spacing and 30 nm nanowire diameter, which results in a low-cost contribution percentage toward TRS net cost.

CONCLUSIONS

The TRS performance in VIS transmittance and mid-IR reflection is comparable to that of the latest transparent personal thermoregulatory textiles, as shown in Table S1. Additionally, the TRS displays a similar temperature difference (7.0 °C). The stretchability, solution processability and materials used for the TRS and earlier discussed references demonstrate our technology's benefits. By using a spray-coating synthesis method, the limiting factor for TRS dimensions becomes the substrate size chosen. It is therefore theoretically possible to create any size or geometrical shape of TRS specimens to conform to any body or object. Stretchability will also guarantee minimal disruption of shielding effects and permit long-term wear. In Figure S9,

the TRS is adhered to personal clothing and is shown to be capable of reducing the composite's emissivity for human body heat suppression. Wash tests were also conducted, showing strong adhesion to fabrics.

Thermal management transparent coatings have been developed with indium tin oxide (ITO).^{44,45} Despite such works, ITO is not the ideal material for wearable technology upscaling, as elevated temperatures or magnetron sputtering methods are necessary for high-quality films, which is expensive and time-consuming. A scalable fabrication approach that does not form bilayers of AgNW networks for smaller nanowire spacing will be required to further improve the transparent radiation shield.

The TRS is a promising approach for thermoregulatory textile coatings as our study focuses on optical theory to guide the fabrication of the AgNW network for ultimate VIS transparency and significant human body heat suppression. Its solution-processing method and incredible stretching capacity also generate opportunities for multiple radiation shielding applications. The TRS may be used to insulate windows for building energy savings with minimal impact on visibility. Applications may also expand to counterfeiting and smart windows. Commercialization of the TRS will produce large energy savings and protect individuals prone to cold injuries.

METHODS/EXPERIMENTAL

Mid-IR simulations of the AgNW mesh screen network are performed using an equivalent sheet impedance operator described by ref 36. The model assumes a single layer of nanowires. Simulations for AgNWs are conducted over a range of 500–10500 nm pore spacings. Visible properties of the AgNW mesh are modeled after the Mie theory. Far-field approximation calculates the radiative properties of 2D infinitely long nanowires. Scattering of AgNWs is once again conducted at the identical pore spacing range previously mentioned. For our purposes, a single-layered, opaque nanowire is sufficient to predict the visible transmission of AgNWs.

Fabrication of the TRS consists of a 20 wt % SEBS in toluene solution drop cast over a glass slide washed prior in isopropyl alcohol sonication for 30 min, followed by a deionized (DI) water sonication wash for another 30 min. The solution is heated on a glass substrate at 65 and 110 °C for 10 min each. Once toluene is evaporated, AgNWs (water solvent) are vacuum filtered through a Buchner funnel flask using a nylon filter with a 0.22 μm pore size. AgNWs with the nylon filter are pasted onto the SEBS film and peeled, leaving behind a AgNW mesh network. A protective topcoat is spray deposited onto the composite using an airbrush gun at 25 PSI and a 5 wt % SEBS solution. A similar heating procedure ensues after spray coating. To further examine the benefits of a SEBS film for the TRS, Sylgard 184 (polydimethylsiloxane elastomer) is fabricated using a similar synthesis procedure to that discussed previously for SEBS. Heating was prolonged for PDMS until fully polymerized. For alternate fabrication methods such as spin-coating, AgNWs are deposited onto a SEBS substrate, and the composite undergoes 30 s of spinning at 1000 rpm and is then dried at 95 °C for 5 min to induce the removal of water.

Wash tests were performed in 100 mL of DI water mixed with 0.7 mL of Tide detergent soap. Multiple stir bars were used to induce vigorous washing of the TRS specimens. Each wash is mixed at 800 rpm for 40 min. Tensile testing was performed on a Zwick Roell zwickLine Z0.5 tensile tester. The TRS specimens were cut according to the ASTM standard dumbbell shape. The TRS specimen dimensions are 26 mm, 4 mm, and 0.15 mm for length, width, and average thickness, respectively, for the dumbbell midsection.

Mid-IR measurements were conducted on a Nicolet iS50 FT-IR spectrometer (Thermo Scientific). The reference sample for mid-infrared measurements is a 100 nm thick Au film on a Si substrate.

Mid-IR reflectance values are computed by the weight average of intensity based on human body temperature (307 K) blackbody radiation via Planck's law. A UV–vis–NIR spectrometer with an integrated sphere (UV-3600 Plus, Shimadzu) was utilized for total visible light transmission. Weight-averaged visible transmission is based on the visible regime 400–800 nm from AM1.5 hemispherical solar radiation (ASTM G-173). Five arbitrary locations were measured and averaged for the final values of each specimen. Specimen haze is measured by diffuse light calculated by removing spectral light from the total measurement.

Scanning electron microscope images were taken with a TESCAN LYRA3 field-emission SEM at the Department of the Geophysical Sciences at the University of Chicago. The transmission electron microscopy image was produced by Dr. Yimei Chen at the Advanced Electron Microscopy Facility at the University of Chicago. Infrared images were taken with a FLIR One Pro thermal camera.

ASSOCIATED CONTENT

Supporting Information

The Supporting Information is available free of charge at <https://pubs.acs.org/doi/10.1021/acsnano.4c02093>.

VIS transmittance and mid-IR reflectance theoretical computational framework (Note 1), derivation of nanowire concentration from porosity (Note 2), weight-average calculation of experimental results (Note 3), comparison of TRS properties with latest research (Table S1), COMSOL VIS forward scattering profiles of a single AgNW (Figure S1), optical and mechanical properties of SEBS, PDMS, and PU (Figure S2), schematic of alternative fabrication methods for the TRS (Figure S3), SEM images and corresponding nanowire spacing estimation of AgNW networks at varying concentrations (Figure S4), SEM images of elongated TRS specimens (Figure S5), tensile testing of TRS samples (Figure S6 and Table S2), cost analysis of the TRS (Note 4, Table S3, and Table S4), haze measurements of AgNW networks when diameter and nanowire spacing vary (Figure S7), UV light exposure tests (Figure S8), TRS adhesion onto personal clothing (Figure S9) (PDF)

Video of the TRS bending (Video S1) (AVI)

Video of the TRS twisting (Video S2) (AVI)

Video of the TRS stretching (Video S3) (AVI)

AUTHOR INFORMATION

Corresponding Author

Po-Chun Hsu – Pritzker School of Molecular Engineering, University of Chicago, Chicago, Illinois 60637, United States; orcid.org/0000-0002-6509-9377; Email: pochunhsu@uchicago.edu

Authors

Genesis Higueros – Pritzker School of Molecular Engineering, University of Chicago, Chicago, Illinois 60637, United States; Thomas Lord Department of Mechanical Engineering and Materials Science, Duke University, Durham, North Carolina 27708, United States; orcid.org/0009-0005-6653-1693

Keyu Wang – Pritzker School of Molecular Engineering, University of Chicago, Chicago, Illinois 60637, United States; School of Mechanical Engineering, Purdue University, West Lafayette, Indiana 47907, United States

Chenxi Sui – Pritzker School of Molecular Engineering, University of Chicago, Chicago, Illinois 60637, United States; orcid.org/0000-0003-2244-8431

Complete contact information is available at:
<https://pubs.acs.org/10.1021/acsnano.4c02093>

Author Contributions

G.H. and K.W. contributed equally to this work. P.-C.H. conceived the concept and supervised the project. K.W. produced the theoretical simulations for VIS and MIR predictions. G.H. and K.W. designed the experimental protocols. G.H. fabricated specimens, interpreted data, and plotted figures. C.S. performed COMSOL simulations and analyzed data results. G.H. wrote the first draft of the manuscript, and all authors revised the paper.

Notes

The authors declare no competing financial interest.

ACKNOWLEDGMENTS

We thank the financial support from the National Science Foundation (ECCS Award No. 2145933).

REFERENCES

- (1) Lee, H.; Calvin, K.; Dasgupta, D.; Krinner, G.; Mukherji, A.; Thorne, P. W.; Trisos, C.; Romero, J.; Aldunce, P.; Barret, K.; et al. *IPCC, 2023: Climate Change 2023: Synthesis Report, Summary for Policymakers. Contribution of Working Groups I, II and III to the Sixth Assessment Report of the Intergovernmental Panel on Climate Change* [Core Writing Team, H. Lee and J. Romero, Eds.]; IPCC: Geneva, Switzerland, 2023; pp 1–34.
- (2) Li, X.; Sun, B.; Sui, C.; Nandi, A.; Fang, H.; Peng, Y.; Tan, G.; Hsu, P.-C. Integration of daytime radiative cooling and solar heating for year-round energy saving in buildings. *Nat. Commun.* **2020**, *11* (1), 6101.
- (3) Wu, R.; Chen, T.-H.; Hsu, P.-C. Stay healthy under global warming: A review of wearable technology for thermoregulation. *EcoMat* **2023**, *5* (10), No. e12396.
- (4) Zuo, X.; Zhang, X.; Qu, L.; Miao, J. Smart Fibers and Textiles for Personal Thermal Management in Emerging Wearable Applications. *Adv. Mater. Technol.* **2023**, *8* (6), No. 2201137.
- (5) Hsu, P.-C.; Liu, X.; Liu, C.; Xie, X.; Lee, H. R.; Welch, A. J.; Zhao, T.; Cui, Y. Personal thermal management by metallic nanowire-coated textile. *Nano Lett.* **2015**, *15* (1), 365–371.
- (6) Liang, L.; Yu, R.; Ong, S. J. H.; Yang, Y.; Zhang, B.; Ji, G.; Xu, Z. J. An Adaptive Multispectral Mechano-Optical System for Multipurpose Applications. *ACS Nano* **2023**, *17* (13), 12409–12421.
- (7) Hsu, P.-C.; Liu, C.; Song, A. Y.; Zhang, Z.; Peng, Y.; Xie, J.; Liu, K.; Wu, C.-L.; Catrysse, P. B.; Cai, L.; et al. A dual-mode textile for human body radiative heating and cooling. *Sci. Adv.* **2015**, *3* (11), No. e1700895.
- (8) Williams, N. Protecting Outdoor workers from Cold. *Occup. Med.* **2023**, *73* (4), 230–230.
- (9) Orton, C.; Gannon, M.; Stewart, B.; Pham, T.; Mesic, A.; Carrougher, G. 760 Building Cold Injury Prevention and Control Strategies with People Who are Experiencing Homelessness. *Journal of Burn Care & Research* **2023**, *44* (Supplement 2), S164–S164.
- (10) Zhu, R.; Wang, J.; Jiang, J.; Xu, C.; Liu, C.; Jia, Y.; Sui, S.; Zhang, Z.; Liu, T.; Chu, Z.; et al. Machine-learning-empowered multispectral metafilm with reduced radar cross section, low infrared emissivity, and visible transparency. *Photon. Res.* **2022**, *10* (5), 1146–1156.
- (11) Dong, X.-X.; Cao, Y.-M.; Wang, C.; Wu, B.; Zheng, M.; Xue, Y.-B.; Li, W.; Han, B.; Zheng, M.; Wang, Z.-S.; Zhuo, M.-P. MXene-Decorated Smart Textiles with the Desired Mid-Infrared Emissivity for Passive Personal Thermal Management. *ACS Appl. Mater. Interfaces* **2023**, *15* (9), 12032–12040.
- (12) Shi, M.; Shen, M.; Guo, X.; Jin, X.; Cao, Y.; Yang, Y.; Wang, W.; Wang, J. Ti₃C₂T_x MXene-Decorated Nanoporous Polyethylene Textile for Passive and Active Personal Precision Heating. *ACS Nano* **2021**, *15* (7), 11396–11405.
- (13) Zhou, Z.; Wang, X.; Ma, Y.; Hu, B.; Zhou, J. Transparent Polymer Coatings for Energy-Efficient Daytime Window Cooling. *Cell Rep. Phys. Sci.* **2020**, *1* (11), No. 100231.
- (14) Fan, J. C. C.; Bachner, F. J.; Foley, G. H.; Zavracky, P. M. Transparent heat-mirror films of TiO₂/Ag/TiO₂ for solar energy collection and radiation insulation. *Appl. Phys. Lett.* **2003**, *25* (12), 693–695.
- (15) Wang, Z.; Yang, H.; Li, Y.; Zheng, X. Robust Silk Fibroin/Graphene Oxide Aerogel Fiber for Radiative Heating Textiles. *ACS Appl. Mater. Interfaces* **2020**, *12* (13), 15726–15736.
- (16) Peng, Y.; Cui, Y. Advanced Textiles for Personal Thermal Management and Energy. *Joule* **2020**, *4* (4), 724–742.
- (17) Liu, X.; Miao, J.; Fan, Q.; Zhang, W.; Zuo, X.; Tian, M.; Zhu, S.; Zhang, X.; Qu, L. Smart Textile Based on 3D Stretchable Silver Nanowires/MXene Conductive Networks for Personal Healthcare and Thermal Management. *ACS Appl. Mater. Interfaces* **2021**, *13* (47), 56607–56619.
- (18) Gao, Q.; Lauster, T.; Kopera, B. A. F.; Retsch, M.; Agarwal, S.; Greiner, A. Breathable and Flexible Dual-Sided Nonwovens with Adjustable Infrared Optical Performances for Smart Textile. *Adv. Funct. Mater.* **2022**, *32* (5), No. 2108808.
- (19) Zhu, Y.; Wang, W.; Zhou, Y.; Qin, B.; Zhou, T.; Qiu, M.; Li, Q. Colored Woven Cloth-Based Textile for Passive Radiative Heating. *Laser Photonics Rev.* **2023**, *17* (11), No. 2300293.
- (20) Kong, M.; Guo, X.; Zhang, S.; Zhang, Y.; Tang, B. Structural colored textiles with high color visibility and stability for intelligent thermoregulating performance. *Chem. Eng. J.* **2023**, *473*, No. 145332.
- (21) Li, W.; Shi, Y.; Chen, Z.; Fan, S. Photonic thermal management of coloured objects. *Nat. Commun.* **2018**, *9* (1), 4240.
- (22) Zhu, Z.; Zhang, J.; Tong, Y.-L.; Peng, G.; Cui, T.; Wang, C.-F.; Chen, S.; Weitz, D. A. Reduced Graphene Oxide Membrane Induced Robust Structural Colors toward Personal Thermal Management. *ACS Photonics* **2019**, *6* (1), 116–122.
- (23) Woo, H. K.; Zhou, K.; Kim, S.-K.; Manjarrez, A.; Hoque, M. J.; Seong, T.-Y.; Cai, L. Visibly Transparent and Infrared Reflective Coatings for Personal Thermal Management and Thermal Camouflage. *Adv. Funct. Mater.* **2022**, *32* (38), No. 2201432.
- (24) Du, X.; Li, X.; Zhang, Y.; Guo, X.; Li, Z.; Cao, Y.; Yang, Y.; Wang, W.; Wang, J. Visible transparent, infrared stealthy polymeric films with nanocoating of ITO@MXene enable efficient passive radiative heating and solar/electric thermal conversion. *Nano Research* **2023**, *16* (2), 3326–3332.
- (25) Hong, S.; Lee, H.; Lee, J.; Kwon, J.; Han, S.; Suh, Y. D.; Cho, H.; Shin, J.; Yeo, J.; Ko, S. H. Highly Stretchable and Transparent Metal Nanowire Heater for Wearable Electronics Applications. *Adv. Mater.* **2015**, *27* (32), 4744–4751.
- (26) Jia, Y.; Liu, D.; Chen, D.; Jin, Y.; Chen, C.; Tao, J.; Cheng, H.; Zhou, S.; Cheng, B.; Wang, X.; et al. Transparent dynamic infrared emissivity regulators. *Nat. Commun.* **2023**, *14* (1), 5087.
- (27) Hu, H.; Wang, S.; Meng, Y.; Liu, G.; Li, M.; Vu, T. D.; Long, Y. Layer-by-Layer Alignment of Silver Nanowires for Transparent and Flexible Energy-Saving Windows. *Adv. Mater. Technol.* **2022**, *7* (3), No. 2100824.
- (28) Lin, S.; Wang, H.; Zhang, X.; Wang, D.; Zu, D.; Song, J.; Liu, Z.; Huang, Y.; Huang, K.; Tao, N.; et al. Direct spray-coating of highly robust and transparent Ag nanowires for energy saving windows. *Nano Energy* **2019**, *62*, 111–116.
- (29) Hanauer, S.; Celle, C.; Crivello, C.; Szabolics, H.; Muñoz-Rojas, D.; Bellet, D.; Simonato, J.-P. Transparent and Mechanically Resistant Silver-Nanowire-Based Low-Emissivity Coatings. *ACS Appl. Mater. Interfaces* **2021**, *13* (18), 21971–21978.
- (30) Baygi, S. J. M. Effect of the Thin Silver Layer in SnO₂/Ag/SnO₂ Nano-Coatings with Low Emission for Energy Storage. *J. Electron. Mater.* **2023**, *52* (7), 4532–4539.
- (31) Bobinger, M.; Angeli, D.; Colasanti, S.; La Torraca, P.; Larcher, L.; Lugli, P. Infrared, transient thermal, and electrical properties of silver nanowire thin films for transparent heaters and energy-efficient coatings. *Phys. Status Solidi (a)* **2017**, *214* (1), No. 1600466.

- (32) Deng, H.-T.; Wen, D.-L.; Liu, J.-R.; Zhang, X.-R.; Wang, Y.-L.; Huang, P.; Kim, B.; Zhang, X.-S. Stretchable multifunctional sensor based on porous silver nanowire/silicone rubber conductive film. *Nano Research* **2023**, *16* (5), 7618–7626.
- (33) Hawkins, S. C. Algorithm 1009: MieSolver—An Object-Oriented Mie Series Software for Wave Scattering by Cylinders. *ACM Trans. Math. Softw.* **2020**, *46* (2), Article 19, 1
- (34) Schäfer, J.; Lee, S. C.; Kienle, A. Calculation of the near fields for the scattering of electromagnetic waves by multiple infinite cylinders at perpendicular incidence. *J. Quant. Spectrosc. Radiat. Transfer* **2012**, *113* (16), 2113–2123.
- (35) Matzler, C. MATLAB Functions for Mie Scattering and Absorption. *IAP Res. Rep.* **2002**, *02* (08).
- (36) Casey, K. F. Electromagnetic shielding behavior of wire-mesh screens. *IEEE Trans. Electromagn. Compat.* **1988**, *30* (3), 298–306.
- (37) Fang, H.; Xie, W.; Li, X.; Fan, K.; Lai, Y.-T.; Sun, B.; Bai, S.; Padilla, W. J.; Hsu, P.-C. A Triple-Mode Midinfrared Modulator for Radiative Heat Management of Objects with Various Emissivity. *Nano Lett.* **2021**, *21* (9), 4106–4114.
- (38) Li, X.; Ma, B.; Dai, J.; Sui, C.; Pande, D.; Smith, D. R.; Brinson, L. C.; Hsu, P.-C. Metalized polyamide heterostructure as a moisture-responsive actuator for multimodal adaptive personal heat management. *Sci. Adv.* **2021**, *7* (51), No. eabj7906.
- (39) Chen, T.-H.; Hong, Y.; Fu, C.-T.; Nandi, A.; Xie, W.; Yin, J.; Hsu, P.-C. A kirigami-enabled electrochromic wearable variable-emittance device for energy-efficient adaptive personal thermoregulation. *PNAS Nexus* **2023**, *2* (6),
- (40) Leung, E. M.; Colorado Escobar, M.; Stiubianu, G. T.; Jim, S. R.; Vyatskikh, A. L.; Feng, Z.; Garner, N.; Patel, P.; Naughton, K. L.; Follador, M.; et al. A dynamic thermoregulatory material inspired by squid skin. *Nat. Commun.* **2019**, *10* (1), 1947.
- (41) Tao, J.; Liu, N.; Li, S.; Shi, J.; Ji, S. Structural manipulation of silver nanowire transparent conductive films for optoelectrical property optimization in different application fields. *Thin Solid Films* **2021**, *729*, No. 138679.
- (42) Kim, Y.; Park, C.; Im, S.; Kim, J. H. Design of intrinsically stretchable and highly conductive polymers for fully stretchable electrochromic devices. *Sci. Rep.* **2020**, *10* (1), 16488.
- (43) Jeon, J. Y.; Park, S.; Han, J.; Maurya, S.; Mohanty, A. D.; Tian, D.; Saikia, N.; Hickner, M. A.; Ryu, C. Y.; Tuckerman, M. E.; et al. Synthesis of Aromatic Anion Exchange Membranes by Friedel–Crafts Bromoalkylation and Cross-Linking of Polystyrene Block Copolymers. *Macromolecules* **2019**, *52* (5), 2139–2147.
- (44) Abd-Elnaiem, A. M.; Hakamy, A. Influence of annealing temperature on structural, electrical, and optical properties of 80 nm thick indium-doped tin oxide on borofloat glass. *J. Mater. Sci.: Mater. Electron.* **2022**, *33* (30), 23293–23305.
- (45) Xu, Y.; Wan, G.; Ma, L.; Zhang, Y.; Su, Y.; Liu, D.; Wang, G. Indium tin oxide as a dual-band compatible stealth material with low infrared emissivity and strong microwave absorption. *J. Mater. Chem. C* **2023**, *11* (5), 1754–1763.